RSC Advances

ROYAL SOCIETY OF CHEMISTRY

www.rsc.org/advances

Design, synthesis, biological evaluation and molecular docking of novel metronidazole derivatives as selective and potent JAK3 inhibitors

Ya-Li Sang†, Yong-Tao Duan†, Han-Yue Qiu, Peng-Fei Wang, Jigar A. Makawana, Zhong-Chang Wang, Hai-Liang Zhu *, Zhen-Xiang He *

State Key Laboratory of Pharmaceutical Biotechnology, Nanjing University, Nanjing 210093, People's Republic of China

*Corresponding authors. Tel. & fax: +86-25-83592672; e-mail: zhuhl@nju.edu.cn, zxhe@nju.edu.cn

†These two authors equally contributed to this paper.

ABSTRACT

In JAK/STAT pathway, sustainable activation of JAK with the capabilities of regulating cell growth and apoptosis can produce abnormal proliferation in tumor cells. A series of novel metronidazole derivatives containing 1,4-benzodioxan moiety as potential inhibitors targeting JAK have been designed, synthesized and their biological activities were also evaluated. Among all synthesized compounds, compound **4t** possessed the most potent antitumor activity against A549, Hela, HepG-2 and U251 *in vitro*, with IC_{50} values of 65, 21, 16 and 44 *n*M, respectively, which has been proved by the result of flow cytometry (FCM) assay. Docking simulation demonstrated that compound **4t** could bind tightly with the crystal structure of JAK3 active site and act as a potential JAK3 inhibitor.

Keywords

Metronidazole derivatives

1,4-benzodioxan

JAK

Molecular docking

Antiproliferative activity

1 Introduction

The JAK/STAT (Janus associated kinase-signal transducer and activator of transcription) pathway involving in signal transduction by transmitting extracellular signals (growth promoting factors, cytokines or hormones) to the nucleus to control gene expression has a prominent part in regulating cell fates, such as cell growth, survival, differentiation, proliferation and apoptosis. Deregulated JAK/STAT signaling which has only recently begun to be explored is intimately linked to tumorigenesis, [1] hematological malignancies, [2] and myeloproliferative disorder. [3] JAK family composed of JAK1-3 and Tyk2 is PTK (protein tyrosine kinase) binding to the juxtamembrane region of cytokine receptors. [4-5] Triggered by dimerization of receptor, which is the result of binding of a ligand with its receptor, JAK will be activated. Subsequently activated JAK phosphorylates STAT, close behind is the dimerization of specific phosphorylated STAT proteins and ensuing activated STATs translocate into the nucleus, regarding as transcription factors to regulate gene expression. [6-7] Following this molecular mechanism (Figure 1), the JAK/STAT3 pathway has been found to be key events in the occurrence, growth and progression of tumors, as well as it may offer us targets for the cancer therapy. [8]

The sustainable activation of STAT3 is required for the development of skin cancer, [9] head and breast tumors [10] *etc*. Furthermore, STAT3 plays a critical role in cancer inflammation and immunity. [11] Since tumorigenesis is a multistage process, activated STAT3 will not lead to cell deformation alone, but is the key inducing factor of tumorigenesis. STAT3, activated by JAK, partners JAK *in vivo*. [12] Consequently, JAK is actively pursued as targets in the research of therapeutic agents, not only against cancer, but also many other diseases by blocking the signal transduction of JAK/STAT3 pathway.

A new phase of targeted therapies is rapidly emerging. Meanwhile, compounds that target PTK are in preclinical and clinical research. These compounds are generally separated into two classes: monoclonal antibodies and small-molecule anti-tumor agents, [13] and the current progress of the small molecules acting as TKIs (tyrosine kinases inhibitors) is promising. [14] During the research of JAK inhibitors, a

host of chemotypes have been designated (Figure 2). [15] Among which, Ruxolitinib (INCB18424) serving as potent and selective JAK inhibitor recently gets approval of FDA, supplying the best available therapy for myelofibrosis, [16] erythrocytosis [17] and other indications [18] by interrupting JAK/STAT signal transduction. Equally as INCB18424, notably, AZD1480, MK0457 also have imidazole ring which has an unequalled place in the field of synthesizing medicine. [19] Imidazole derivatives are active against bacteria, viruses, fungi and some imidazole drugs have anticancer properties. Particularly, imidazole ring is capable of high specificity, selectivity and affinity bonding to proteins by hydrogen bonds or metals as a ligand and drugs, [20] which has been demonstrated by the following docking simulations. Meanwhile, within 1,4-benzodioxan, the oxygen at location 4 maintains the stability of an optimum conformation for drug-receptor interaction complexes. On the other hand, the oxygen at location 1 contributes to the binding by interacting with receptor polar pockets, [21] which also occurs in our docking simulations. Moreover, 1,4-benzodioxan derivatives reveal powerful biological activities (anticancer, [22] anti-fungal and antipsychotic activities [23]). For example, 1,2,4-triazoles having 1,4-benzodioxan (A) fragments was synthesized as potential MetAP2 inhibitors, [22] WB 4101 (B) were regarded as subtype-selective alpha1-adrenoreceptor antagonists (Figure 3). [24]

Furthermore, our research team has already made some progress in the research of imidazole derivatives as TKIs. [25-26] All of these inspire us to do further research in the direction of finding new imidazole derivatives containing 1,4-benzodioxan moiety as promising TKIs. Herein we depict the synthesis, antitumor activity, succeeding structure activity relationship (SAR) and Flow Cytometry (FCM) studies of target compounds. Docking simulations are also accomplished by binding the X-ray crystallographic structure of the JAK3 with inhibitors to predict the binding modes and affinity.

2. Result and discussion

2.1. Chemistry

The synthetic routes of a series of novel metronidazole derivatives including 1,4-benzodioxan moiety targeting JAK (**4a-4u**) were outlined in Scheme 1A. First of

all, different substituted (*E*)-2-(5-nitro-2-styryl-1*H*-imidazol-1-*yl*)ethan-1-ol (**2a-2u**) were synthesized by reaction of metronidazole with diverse substituted benzaldehydes in DMSO with the presence of sodium methylate as catalyst. Compounds **2a-2u** were converted into different substituted (*E*)-2-(5-Nitro-2-styryl-1*H*-imidazol-1-*yl*)ethyl 4-methylbenzenesufonate (**3a-3u**) by reaction with 4-toluene sulfonyl chloride using triethylamine as promoter in CH_2Cl_2 at room temperature in high yield. Finally, compounds **3a-3u** and 1,4-benzodioxan were dissolved in DMF under a refluxing and K_2CO_3-base condition, stirring together the reactants to an adequate degree. The target compounds could be obtained with yields in the range of 60-80%. Meanwhile, the desired products could be produced following another pathway outlined in Scheme 1B. Initially, treat 1,4-benzodioxan in refluxing thionyl chloride with a few drops of DMF for 4 h to get 2,3-dihydrobenzo[*b*][1,4]dioxine-5-carbonyl chloride (**6**). Then, different substituted (*E*)-2-(5-nitro-2-styryl-1*H*-imidazol-1-*yl*)ethyl 2,3-dihydrobenzo[*b*][1,4]dioxine-6-carboxylate (**4a-4u**) were synthesized in CH_2Cl_2 by treating compounds **3a-3u** with solution of compound **6** in CH_2Cl_2 dropwise using triethylamine as promoter in high yield.

2.2. Bioassay

2.2.1. Antitumor assay

In order to test the biological activities of the two series of novel metronidazole derivatives (**3a-3u** and **4a-4u**), compared to the potent positive control tofacitinib citrate *in vitro*, we evaluated their anti-proliferative abilities against four cultured cell lines, which were adenocarcinomic human alveolar basal epithelial cells A549, human glioma cells U251, human hepatocellular liver carcinoma cell line HepG-2 and human cervical cancer cell line Hela. The IC_{50} results of **3a-3u** and **4a-4u** were illustrated in Table 1 and Table 2, respectively. It was observed that the compounds which consist of 1,4-benzodioxan moiety (**4a-4u**) showed notable anticancer effects and superior antitumor activities in comparison to **3a-3u.** For example, among four cell lines, the Hela activities demonstrated inhibition constant (IC_{50}) values between 18 and 177 *n*M in Table 2, compared to 0.52 and 9.68 μM in Table 1.

As depicted in Table 2, among these compounds, compound **4t** has the most effective anti-proliferative ability (IC_{50} = 21 *n*M for Hela and IC_{50} = 44 *n*M for U251) in comparison to the positive control tofacitinib citrate (IC_{50} = 5 *n*M for Hela and IC_{50} = 27 *n*M for U251). Hela was found to display higher sensitivity toward these compounds than other cell lines. Nevertheless, A549 was observed to be relatively poor sensitive toward them with IC_{50} ranging from 65 to 744 *n*M. Regarding HepG-2, compounds **4d** and **4t** particularly revealed potent inhibiting effect (IC_{50} = 76 and 16 *n*M, respectively), compared to tofacitinib citrate (12 *n*M).

The ensuing structure-activity relationship (SAR) can be observed by the different JAK inhibitory activities of these compounds with varying substituted parts in Table 1 and Table 2. By and large, the inhibitory abilities of 1,4-benzodioxan derivatives (**4a-4u**) became much better than **3a-3u**. Primarily, to these compounds, Structure activity relationship (SAR) study showed that stronger electron-withdrawing substitute has better JAK inhibitory activities (*e.g.* **4b, 4e, 4h, 4k, 4n, 4q**), whereas the difference was slight. Besides, we proceeded to detect the molecular docking of potent antitumor agents (**4d**, **4f**, **4t)** with the JAK3 crystal structure (PDB code: 3FUP). All docking programs were operated by Discovery Studio 3.5. The binding models of inhibitors (**4d**, **4f**, **4t)** with 3FUP were illustrated in Figure 4. In figure 4C, benzene ring containing two electron-withdrawing halogen atoms tightly bound to 3FUP via one π-π interaction and one π-sigma interaction. Meanwhile, the two chlorine atoms of **4t** interacted with amino acid residues of JAK3 by electrostatic interactions, van der waals and covalent bonds. While, in figure 4A and 4B, one-substituted chlorine atom occupied smaller space and displayed weaker electronegativity compared to di-substituted moieties. The molecular docking results revealed that compound **4t** bound stronger to 3FUP than **4d** and **4f**. The antitumor activities showed compounds with di-substituted moieties (*e.g.* **4t**, **4s**) indicated more improved antitumor activities than those with one-substituted atom (*e.g.* **4d, 4f**). According to SAR analysis, the active gradient was 2,4-2Cl **>** 2-Cl-6-F **>** -F **>** -Cl **>** -Br **>** $-OCH_3$ **>** $-CH_3$ **>** H **>** $-NO_2$. Moreover, a meta substitute (**4e**) had improved

antitumor activity comparing to the ortho (**4d**) or para (**4f**) position. The foregoing SAR analysis showed that compounds **4t** was the most effective JAK inhibitory agent, meanwhile, other compounds were also found to be potent inhibitors because of their effective antitumor activities, compared to the potent positive control tofacitinib citrate.

2.2.2. JAK3 inhibitory activity

The JAK3 inhibitory abilities of compounds **4a**-**4u** were evaluated using a solid-phase ELISA assay and the results were illustrated in Table 2. All synthesized compounds displayed obviously JAK3 inhibitory activity with IC_{50} values ranging from 9 and 102 *n*M.

2.2.3. Detection of apoptosis by flow cytometry (FCM)

With apoptosis of cancer cells，the damage to body would be generally eliminated. In order to test whether these compounds inhibited tumor growth by inducing apoptosis, we researched the mechanism of anticancer activity of compound **4t** by Annexin V-PE fluorescence-activated cell sorting (FACS) using FCM. HELA cells were cultured *in vitro* treated with a gradient concentration (0, 6, 18, 54 *n*M) of **4t** for 24 h. By analyzing the results of this experiment, the apoptotic rate of cell ranging from 20.0% to 58.1% versus control 4.6% demonstrated that compound **4t** could induce the apoptosis of activated HELA cells in a density-dependent manner at 24 h (Figure 5).

2.3. Molecular docking study

All our present efforts have been directed towards gaining better understanding on the effectiveness of the synthesized compounds and guiding further SAR studies. In order to achive this goal, we proceeded to detect the molecular docking of potent antitumor agents (**3t**, **4t)** with the JAK3 crystal structure (PDB code: 3FUP). All docking programs were operated by Discovery Studio 3.5. The binding models of inhibitors (**3t**, **4t)** with 3FUP were illustrated in Figure 6. The amino acid residues which bound with 3FUP were labeled. In the binding mode (Figure 6B), compound **4t** nicely bound to 3FUP via three hydrogen bonds, one π-π interaction, one π-sigma

interaction and other interactions (*e.g.*, electrostatic interaction, van der waals). One oxygen atom on the triazole ring with ARG938 (distance N-O…H = 4.5 Å) and the nitrogen atom of -NO_2 with ASP939 (distance O-N…H = 5.5 Å) made important contributions to the hydrogen bonding interaction. The third hydrogen bond was formed by oxygen atom on the 1,4-benzodioxan ring with ARG980 (distance H-O…H = 4.7 Å), together with the above two hydrogen bonds, being a probable crucial factors for its potent activity. In addition, the π-π interaction and π-sigma interaction were formed between the benzene ring and LEU855 (distance = 2.9 Å), TYR931 (distance = 6.3 Å), respectively. Besides, the binding model was enhanced by electrostatic interaction formed between compound **4t** and residues (*e.g.* LYS857, LEU932, ASN981) and van der waals formed by compound **4t** and residues (*e.g.* GLY935, VAL863, ASP976). Meanwhile, it was observed that the potent inhibitor **4t** was retained tightly by the binding pocket of 3FUP, from the receptor surface model in Figure 6C. However, in Figure 6A, compound **3t** bound to 3FUP via two π-cation interactions and other interactions (*e.g.* electrostatic interaction, van der waals). These molecular docking results showed that, compare the common structural part of **3t** and **4t**, the latter bound stronger to JAK3. Along with the bioassay data, the docking results revealed that compound **4t** was potential JAK3 inhibitor.

2.4. 3D-QSAR

To obtain a systematic SAR profile on synthesized compounds as JAK3 inhibitors and explore more powerful and selective dual antitumor agents, 21 compounds with accurate IC_{50} values against JAK3 were chosen as the model dataset to build 3D-QSAR model by create-in QSAR software of DS 3.5 (Discovery Studio 3.5, Accelrys, Co. Ltd). In general, the pIC_{50} scale (-logIC_{50}) was transformed from the acquired IC_{50} (μM) values of these synthesized compounds and used as a means in 3D-QSAR model to select activity conformations of the designed molecules and reasonably measure the synthesized antitumor agents. Illustrated in Table 3, the training and test set was randomly selected in due proportion that ratio of training set was 0.762, ratio of test set was 0.238 by the Diverse Molecules method of Discovery

Studio 3.5. The success of this model relied on the acceptable study of docking protocol and bioassay results.

Among the twenty docked poses, the alignment conformation of each molecule owning the lowest CDOCKER_INTERACTION_ENENGY was maintained in default situation. The 3D-QSAR model built by DS 3.5, clarified the crucial regions (steric or electrostatic) affecting the binding affinities. It was a PLS model set up 210 independent variables (conventional R^2 = 0.8396). The experimental and predicted pIC_{50} values and relative residual values of the training set and test set molecules in 3D-QSAR model had been showed in Table 3. Moreover, the graphical relationship of actual and predicted values had been demonstrated in Figure 7A, in which the plot of the actual IC_{50} versus the predicted values proved that this model was reliable in forecasting of activity for metronidazole derivatives containing 1,4-benzodioxan moiety.

A outline plot of the electrostatic field region favorable (in blue) or unfavorable (red) for antitumor activity based on JAK3 protein target were illustrated in Figure 7B, while the energy grids corresponding to the favorable (in green) or unfavorable (yellow) steric effects for the JAK3 affinity were shown in Figure 7C. It was widely acceptable that a better inhibitor based on the 3D-QSAR model should have strong Van der Waals attraction in the green areas and a polar group in the blue electrostatic potential areas (which were dominant close to the skeleton). As shown in these two pictures, this promising model would provide a guideline to design and optimize more effective JAK3 inhibitors based on the metronidazole derivatives containing 1,4-benzodioxan moiety and pave the way for us to further study in future.

3. Conclusion:

Summarily, we have designed and synthesized a novel series of metronidazole derivatives containing 1,4-benzodioxan moiety and evaluated their inhibitory activities against A549, Hela, U251 and HepG-2. Preliminary results illustrated that these compounds showed a promising prospect as antiproliferative agents. Among all compounds, compound **4t** displayed potent biological activities (IC_{50} = 21 *n*M for Hela, IC_{50} = 44 *n*M for U251, IC_{50} = 16 *n*M for HepG-2 and IC_{50} = 65 *n*M for A549),

which had been demonstrated by analysis of apoptosis using flow cytometry (FCM).

Docking simulation provided further insight into the probable binding models and poses between the JAK3 protein and its ligand. It was observed that three hydrogen bonds, one π-π interaction, one π-sigma interaction and other interactions (*e.g.*, electrostatic interaction, van der waals) formed between compound **4t** with the protein residues might play critical roles in its anticancer activities. The results showed that compound **4t** as well as the other metronidazole derivatives has the potential to be selective and potent JAK inhibitor. Eventually, QSAR models had been created on the basis of previous antitumor assay and molecular docking study to offer a reliable tool for reasonable design of JAK inhibitors in future. The information of this QSAR study might help to search more promising anticancer agents.

4. Experiments

4.1. Materials and measurements

All chemicals utilized in present research were of analytical grade. Thin layer chromatography (TLC) was accomplished on silica gel plates (Silica Gel 60 GF254), the result could clearly be seen in UV light (254 nm). Purification of the desired products was performed by column chromatography. The amount of silica gel used in column chromatography was 50-100 times the weight charged on the column. Melting points were determined on a XT4 MP apparatus (Taike Corp, Beijing, China). All the ^{1}H NMR spectra were recorded on a Bruker DPX 300 model Spectrometer in DMSO-d_6 at 25 °C with TMS and chemical shifts (δ) were reported in parts per million (ppm). Elemental analyses were satisfactorily performed on a CHN-O-Rapid instrument within ±0.4% of the theoretical values.

4.2. General procedure for the synthesis of (2-methyl-5-nitro-1*H*-imidazol-1-*yl*)methanol derivatives

A. General procedure for the Synthesis of 2-(5-nitro-2-styryl-1*H*-imidazol-1-***yl***)ethan-1-ol **(2a-2u)**

Metronidazole (10 mmol, 0.82 g) and variety of benzaldehydes (10 mmol) in dimethyl sulfoxide (10 mL) were treated with solution of sodium methylate (8.9 mmol, 0.48 g) in methanol (1 mL) dropwise at room temperature for ten hours. The

reaction was monitored by thin layer chromatography (TLC). Considerable amount of solid product would immediately form after washed with water. Then, the crude products were purified by recrystallization with ethanol, acetone and petroleum ether (2:1:5) washed by ice-water (25 mL) for three times and dried to obtain pure solid products.

B. General procedure for the Synthesis of 2-(5-nitro-2-styryl-1*H*-imidazol-1-*yl*)ethyl 4-methylbenzenesulfonate **(3a-3u)**

To a stirred mixture of compounds **(2a-2u)** (7 mmol) in CH_2Cl_2 (15 mL) were added *p*-methyl benzene sulfonic chloride (7 mmol, 1.53 g) and triethylamine (10 mL) at room temperature, stirring for seven hours. The precipitate was purified by column chromatograghy over silica gel to gain compounds **(3a-3u)**.

C. General procedure for the Synthesis of 2-(5-nitro-2-styryl-1*H*-imidazol-1-*yl*)ethyl 2,3-dihydrobenzo [*b*][1,4] dioxine-6-carboxylate **(4a-4u)**

Compounds **(3a-3u)** (1 mmol) and 1,4-benzodioxan-6- carboxylic acid (1.5 mmol, 0.34 g) were dissolved in DMF (10 mL) under refluxing and K_2CO_3 (5 mmol, 0.69 g)-promoter condition, stirring the reactants together to an adequate degree overnight. The precipitate was filtered and purified by recrystallization to obtain compounds **(4a-4u)**.

4.2.1. 2-(2-(2-Fluorostyry)-5-nitro-1*H*-imidazol-1-*yl*)ethyl 2,3-dihydrobenzo[*b*][1,4]dioxine -5 - carboxylate (4a)

Yellow powder, yield: 65.2%. m.p. 176 ~ 177 ˚C; ^{1}H NMR (DMSO-d_6, 300 MHz, δ ppm): 4.13 (s, 4H, O-CH_2-CH_2-O), 4.58 (t, J = 6.2 Hz, 2H, N-CH_2-C), 5.02 (s, 2H, C-CH_2-O), 6.50 (t, J = 3.6 Hz, 1H, C-CH-C), 6.91 (d, J = 8.4 Hz, 1H, C-CH-C), 7.05~7.31 (m, 5H, Ph-H), 7.79~7.95 (m, 2H, Ph-H), 8.23 (s, 1H, N-CH). MS (ESI): 440.12 ([M+H]$^+$). Anal. Calcd for $C_{22}H_{18}FN_3O_6$: C, 60.14; H, 4.13; N, 9.56; O, 21.85%. Found: C, 60.17; H, 4.08; N, 9.63; O, 21.78%.

4.2.2. 2-(2-(3-Fluorostyry)-5-nitro-1*H*-imidazol-1-*yl*)ethyl 2,3-dihydrobenzo[*b*][1,4]dioxine -5 - carboxylate (4b)

Yellow powder, yield: 58.0%. m.p. 198 ~ 200 ˚C; ^{1}H NMR (DMSO-d_6, 300 MHz, δ ppm): 4.12 (d, J = 5.3 Hz, 4H, O-CH_2-CH_2-O), 4.61 (s, 2H, N-CH_2-C), 5.01 (s, 2H,

C-CH_2-O), 6.58 (d, J = 8.1 Hz, 1H, C-CH-C), 7.16~7.32 (m, 3H, C-CH-C, Ph-H), 7.37~7.55 (m, 3H, Ph-H), 7.59~7.75 (m, 2H, Ph-H), 8.24 (s, 1H, N-CH). MS (ESI): 440.12 ($[M+H]^+$). Anal. Calcd for $C_{22}H_{18}FN_3O_6$: C, 60.14; H, 4.13; N, 9.56; O, 21.85%. Found: C, 60.23; H, 4.04; N, 9.63; O, 21.73%.

4.2.3. 2-(2-(4-Fluorostyry)-5-nitro-1*H*-imidazol-1-*yl*)ethyl 2,3-dihydrobenzo[*b*][1,4]dioxine -5 - carboxylate (4c)

Yellow powder, yield: 64.1%. m.p. 201 ~ 203 ˚C; ^{1}H NMR (DMSO-d_6, 300 MHz, δ ppm): 4.09 (s, 4H, O-CH_2-CH_2-O), 4.60 (s, 2H, N-CH_2-C), 5.00 (s, 2H, C-CH_2-O), 6.57 (d, J = 7.4 Hz, 1H, C-CH-C), 7.14~7.47 (m, 4H, C-CH-C, Ph-H), 7.42~7.66 (m, 2H, Ph-H), 7.70~7.94 (m, 2H, Ph-H), 8.23 (s, 1H, N-CH). MS (ESI): 440.12 ($[M+H]^+$). Anal. Calcd for $C_{22}H_{18}FN_3O_6$: C, 60.14; H, 4.13; N, 9.56; O, 21.85%. Found: C, 60.05; H, 4.18; N, 9.64; O, 21.89%

4.2.4. 2-(2-(2-Chlorostyryl)-5-nitro-1*H*-imidazol-1-*yl*)ethyl 2,3-dihydrobenzo[*b*][1,4]dioxine-5-carboxylate (4d)

Yellow powder, yield: 65.3%. m.p. 181 ~ 182 ˚C; ^{1}H NMR (DMSO-d_6, 300 MHz, δ ppm): 4.07~4.18 (m, 4H, O-CH_2-CH_2), 4.61 (s, 2H, N-CH_2-C), 5.01 (s, 2H, C-CH_2-O), 6.59 (d, J = 7.5 Hz, 1H, C-CH-C), 7.16~7.32 (m, 4H, C-CH-C, Ph-H), 7.32~7.43 (m, 2H, Ph-H), 7.50 (t, J = 4.9 Hz, 2H, Ph-H), 8.24 (s, 1H, N-CH). MS (ESI): 456.09 ($[M+H]^+$). Anal. Calcd for $C_{22}H_{18}ClN_3O_6$: C, 57.97; H, 3.98; N, 9.22; O, 21.06%. Found: C, 57.84; H, 3.91; N, 9.32; O, 21.17%.

4.2.5. 2-(2-(3-Chlorostyryl)-5-nitro-1*H*-imidazol-1-*yl*)ethyl 2,3-dihydrobenzo[*b*][1,4]dioxine-5-carboxylate (4e)

Yellow powder, yield: 59.2%. m.p. 190 ~ 192 ˚C; ^{1}H NMR (DMSO-d_6, 300 MHz, δ ppm): 4.06 (s, 2H, O-CH_2-C), 4.13~4.17 (m, 2H, C-CH_2-O), 4.57 (s, 2H, N-CH_2-C), 5.03 (s, 2H, C-CH_2-O), 6.54 (d, J = 7.3 Hz, 1H, C-CH-C), 7.19~7.35 (m, 4H, C-CH-C, Ph-H), 7.39 (d, J = 5.7 Hz, 3H, Ph-H), 7.69 (t, J = 6.7 Hz, 1H, Ph-H), 8.23 (s, 1H, N-CH). MS (ESI): 456.09 ($[M+H]^+$). Anal. Calcd for $C_{22}H_{18}ClN_3O_6$: C, 57.97; H, 3.98; N, 9.22; O, 21.06%. Found: C, 58.14; H, 3.83; N, 9.07; O, 21.23%.

4.2.6. 2-(2-(4-Chlorostyryl)-5-nitro-1*H*-imidazol-1-*yl*)ethyl 2,3-dihydrobenzo[*b*][1,4]dioxine-5-carboxylate (4f)

Yellow powder, yield: 61.8%. m.p. 206 ~ 208 ˚C; ^{1}H NMR (DMSO-d_6, 300 MHz, δ ppm): 4.07 (s, 2H, O-CH_2-C), 4.17 (s, 2H, O-CH_2-C), 4.59 (s, 2H, N-CH_2-C), 4.99 (s, 2H, C-CH_2-O), 6.58 (d, J = 7.1 Hz, 1H, C-CH-C), 7.22 (t, J = 8.7 Hz, 2H, C-CH-C, Ph-H), 7.45 (t, J = 6.1 Hz, 3H, Ph-H), 7.70 (t, J = 6.3 Hz, 3H, Ph-H), 8.24 (s, 1H, N-CH). MS (ESI): 456.09 ([M+H]$^+$). Anal. Calcd for $C_{22}H_{18}ClN_3O_6$: C, 57.97; H, 3.98; N, 9.22; O, 21.06%. Found: C, 57.91; H, 4.09; N, 9.29; O, 20.92%.

4.2.7. 2-(2-(2-Bromostyryl)-5-nitro-1*H*-imidazol-1-*yl*)ethyl 2,3-dihydrobenzo[*b*][1,4]dioxine-5-carboxylate (4g)

Yellow powder, yield: 65.1%. m.p. 194 ~ 196 ˚C; ^{1}H NMR (DMSO-d_6, 300 MHz, δ ppm): 4.09 (s, 2H, O-CH_2-C), 4.18 (s, 2H, O-CH_2-C), 4.59 (s, 2H, N-CH_2-C), 5.01 (s, 2H, C-CH_2-O), 6.67 (d, J = 7.0 Hz, 1H, C-CH-C), 7.21 (t, J = 8.7 Hz, 2H, C-CH-C, Ph-H), 7.32~7.48 (m, 3H, Ph-H), 7.64~7.85 (m, 3H, Ph-H), 8.25 (s, 1H, N-CH). MS (ESI): 500.04 ([M+H]$^+$). Anal. Calcd for $C_{22}H_{18}BrN_3O_6$: C, 52.82; H, 3.63; N, 8.40; O, 19.19%. Found: C, 52.74; H, 3.57; N, 8.48; O, 19.06%.

4.2.8. 2-(2-(3-Bromostyryl)-5-nitro-1*H*-imidazol-1-*yl*)ethyl 2,3-dihydrobenzo[*b*][1,4]dioxine-5-carboxylate (4h)

Yellow powder, yield: 66.5%. m.p. 193 ~ 195 ˚C; ^{1}H NMR (DMSO-d_6, 300 MHz, δ ppm): 4.12 (s, 4H, O-CH_2-CH_2-O), 4.53 (s, 2H, N-CH_2-C), 5.03 (s, 2H, C-CH_2-O), 6.59 (d, J = 7.4 Hz, 1H, C-CH-C), 7.31~7.47 (m, 4H, C-CH-C, Ph-H), 7.52~7.64 (m, 2H, Ph-H), 7.75~7.81 (m, 2H, Ph-H), 8.25 (s, 1H, N-CH). MS (ESI): 500.04 ([M+H]$^+$). Anal. Calcd for $C_{22}H_{18}BrN_3O_6$: C, 52.82; H, 3.63; N, 8.40; O, 19.19%. Found: C, 52.76; H, 3.73; N, 8.51; O, 19.07%.

4.2.9. 2-(2-(4-Bromostyryl)-5-nitro-1*H*-imidazol-1-*yl*)ethyl 2,3-dihydrobenzo[*b*][1,4]dioxine-5-carboxylate (4i)

Yellow powder, yield: 57.4%. m.p. 205 ~ 207 ˚C; ^{1}H NMR (DMSO-d_6, 300 MHz, δ ppm): 4.24 (s, 4H, O-CH_2-CH_2-O), 4.60 (s, 2H, N-CH_2-C), 5.00 (s, 2H, C-CH_2-O), 6.60 (d, J = 8.4 Hz, 1H, C-CH-C), 7.15~7.29 (m, 2H, C-CH-C, Ph-H), 7.44~7.71 (m, 6H, Ph-H), 8.23 (s, 1H, N-CH). MS (ESI): 500.04 ([M+H]$^+$). Anal. Calcd for $C_{22}H_{18}BrN_3O_6$: C, 52.82; H, 3.63; N, 8.40; O, 19.19%. Found: C, 52.94; H, 3.52; N, 8.48; O, 19.13%.

4.2.10. 2-(2-(2-Methystyryl)-5-nitro-1*H*-imidazol-1-*yl*)ethyl 2,3-dihydrobenzo[*b*][1,4]dioxine-5-carboxylate (4j)

Yellow powder, yield: 72.6%. m.p. 172 ~ 174 ˚C; ^{1}H NMR (DMSO-d_6, 300 MHz, δ ppm): 2.50 (s, 3H, -CH_3), 4.13 (d, J = 6.0 Hz, 4H, O-CH_2-CH_2-O), 4.63 (s, 2H, N-CH_2-C), 4.90 (s, 2H, C-CH_2-O), 6.64 (d, J = 7.3 Hz, 1H, C-CH-C), 7.17~7.46 (m, 7H, C-CH-C, Ph-H), 7.84 (d, J = 5.7 Hz, 1H, Ph-H), 8.27 (s, 1H, N-CH). MS (ESI): 436.14 ([M+H]$^+$). Anal. Calcd for $C_{23}H_{21}N_3O_6$: C, 63.44; H, 4.86; N, 9.65; O, 22.05%. Found: C, 63.35; H, 4.89; N, 9.77; O, 21.99%.

4.2.11. 2-(2-(3-Methystyryl)-5-nitro-1*H*-imidazol-1-*yl*)ethyl 2,3-dihydrobenzo[*b*][1,4]dioxine-5-carboxylat (4k)

Yellow powder, yield: 71.2%. m.p.173 ~ 175 ˚C; ^{1}H NMR (DMSO-d_6, 300 MHz, δ ppm): 2.47 (s, 3H, -CH_3), 4.15 (s, 4H, O-CH_2-CH_2-O), 4.61 (d, J = 4.6 Hz, 2H, N-CH_2-C), 4.92 (t, J = 5.3 Hz, 2H, C-CH_2-O), 6.89 (d, J = 7.3 Hz, 1H, C-CH-C), 7.05~7.34 (m, 2H, C-CH-C, Ph-H), 7.34~7.86 (m, 6H, Ph-H), 8.24 (s, 1H, N-CH). MS (ESI): 436.14 ([M+H]$^+$). Anal. Calcd for $C_{23}H_{21}N_3O_6$: C, 63.44; H, 4.86; N, 9.65; O, 22.05%. Found: C, 63.36; H, 4.97; N, 9.65; O, 21.98%.

4.2.12. 2-(2-(4-Methystyryl)-5-nitro-1*H*-imidazol-1-*yl*)ethyl 2,3-dihydrobenzo[*b*][1,4]dioxine-5-carboxylate (4l)

Yellow powder, yield: 71.4%. m.p. 183 ~ 185 ˚C; ^{1}H NMR (DMSO-d_6, 300 MHz, δ ppm): 2.49 (s, 3H, -CH_3), 4.12 (s, 4H, O-CH_2-CH_2-O), 4.58 (t, J = 4.2 Hz, 2H, N-CH_2-C), 4.87 (t, J = 8.4 Hz, 2H, C-CH_2-O), 6.57 (d, J = 5.3 Hz, 1H, C-CH-C), 6.88~7.15 (m, 2H, C-CH-C, Ph-H), 7.34~7.48 (m, 4H, Ph-H), 7.82~7.98 (m, 2H, Ph-H), 8.27 (s, 1H, N-CH). MS (ESI): 436.14 ([M+H]$^+$). Anal. Calcd for $C_{23}H_{21}N_3O_6$: C, 63.44; H, 4.86; N, 9.65; O, 22.05%. Found: C, 63.33; H, 4.98; N, 9.67; O, 22.13%.

4.2.13. 2-(5-Nitro-2-(2-nitrostyryl)-1*H*-imidazol-1-*yl*)ethyl 2,3-dihydrobenzo[*b*][1,4]dioxine-5-carboxylate (4m)

Yellow powder, yield: 64.4%. m.p.193 ~ 194 ˚C; ^{1}H NMR (DMSO-d_6, 300 MHz, δ ppm): 3.37 (s, 2H, O-CH_2-CH_2), 4.02 (m, 2H, O-CH_2-CH_2), 4.48 (d, J = 6.3 Hz, 2H, N-CH_2-C), 5.04 (s, 2H, C-CH_2-O), 6.84 (d, J = 5.4 Hz, 1H, C-CH-C), 7.27~7.49 (m, 4H, C-CH-C, Ph-H), 7.88~8.35 (m, 4H, Ph-H N-CH), 8.47 (s, 1H, Ph-H). MS (ESI):

467.11 ([M+H]$^+$). Anal. Calcd for $C_{22}H_{18}N_4O_8$: C, 56.65; H, 3.89; N, 12.01; O, 27.44%. Found: C, 56.54; H, 3.94; N, 12.07; O, 27.46%.

4.2.14. 2-(5-Nitro-2-(3-nitrostyryl)-1*H*-imidazol-1-*yl*)ethyl 2,3-dihydrobenzo[*b*][1,4]dioxine-5-carboxylate (4n)

Yellow powder, yield: 58.2%. m.p. 195 ~ 197 ˚C; ^{1}H NMR (DMSO-d_6, 300 MHz, δ ppm): 3.96~4.15 (m, 4H, O-CH_2-CH_2), 4.64 (s, 2H, N-CH_2-C), 5.03 (s, 2H, C-CH_2-O), 6.57 (d, J = 6.5 Hz, 1H, C-CH-C), 7.17~7.28 (m, 2H, C-CH-C, Ph-H), 7.61~7.83 (m, 3H, Ph-H), 8.30~8.56 (m, 3H, Ph-H, N-CH), 8.58 (s, 1H, Ph-H). MS (ESI): 467.11 ([M+H]$^+$). Anal. Calcd for $C_{22}H_{18}N_4O_8$: C, 56.65; H, 3.89; N, 12.01; O, 27.44%. Found: C, 56.74; H, 3.81; N, 11.95; O, 27.53%.

4.2.15. 2-(5-Nitro-2-(4-nitrostyryl)-1*H*-imidazol-1-*yl*)ethyl 2,3-dihydrobenzo[*b*][1,4]dioxine-5-carboxylate (4o)

Yellow powder, yield: 60.1%. m.p. 201 ~ 203 ˚C; ^{1}H NMR (DMSO-d_6, 300 MHz, δ ppm): 3.98~4.18 (m, 4H, O-CH_2-CH_2), 4.57 (s, 2H, N-CH_2-C), 5.01 (s, 2H, C-CH_2-O), 6.63 (d, J = 5.4 Hz, 1H, C-CH-C), 7.07~7.19 (m, 2H, C-CH-C, Ph-H), 7.43~7.54 (m, 4H, Ph-H), 8.27~8.46 (m, 2H, Ph-H, N-CH), 8.42 (s, 1H, Ph-H). MS (ESI): 467.11 ([M+H]$^+$). Anal. Calcd for $C_{22}H_{18}N_4O_8$: C, 56.65; H, 3.89; N, 12.01; O, 27.44%. Found: C, 56.59; H, 3.94; N, 12.07; O, 27.48%.

4.2.16. 2-(2-(2-Methoxystyryl)-5-nitro-1*H*-imidazol-1-*yl*)ethyl 2,3-dihydrobenzo[*b*][1,4]dioxine-5-carboxylat (4p)

Yellow powder, yield: 64.3%. m.p. 178 ~ 179 ˚C; ^{1}H NMR (DMSO-d_6, 300 MHz, δ ppm): 3.77 (s, 3H, C-OCH_3), 4.07~4.09 (m, 2H, O-CH_2-C), 4.17~4.20 (m, 2H, C-CH_2-O), 4.60 (t, J = 7.2 Hz, 2H, N-CH_2-C), 5.00 (t, J = 4.8 Hz, 2H, C-CH_2-O), 6.56 (d, J = 3.9 Hz, 1H, C-CH-C), 6.94~6.97 (m, 1H, C-CH-C), 7.22~7.33 (m, 5H, Ph-H), 7.43 (d, J = 8.2 Hz, 1H, Ph-H), 7.69 (d, J = 7.4 Hz, 1H, Ph-H), 8.23 (s, 1H, N-CH). MS (ESI): 452.14 ([M+H]$^+$). Anal. Calcd for $C_{23}H_{21}N_3O_7$: C, 61.19; H, 4.69; N, 9.31; O, 24.81%. Found: C, 61.08; H, 4.42; N, 9.37; O, 24.93%.

4.2.17. 2-(2-(3-Methoxystyryl)-5-nitro-1*H*-imidazol-1-*yl*)ethyl 2,3-dihydrobenzo[*b*][1,4]dioxine-5-carboxylate (4q)

Yellow powder, yield: 61.3%. m.p. 176 ~ 178 ˚C; ^{1}H NMR (DMSO-d_6, 300 MHz, δ

ppm): 3.76 (s, 3H, C-OCH_3), 4.11 (s, 4H, O-CH_2-CH_2-O), 4.55 (s, 2H, N-CH_2-C), 4.98 (s, 2H, C-CH_2-O), 6.49 (t, *J* = 7.2 Hz, 1H, C-CH-C), 6.92 (t, *J* = 8.4 Hz, 2H, C-CH-C, Ph-H), 7.1 (d, *J* = 5.22 Hz, 1H, Ph-H), 7.32~7.44 (m, 4H, Ph-H), 7.70 (d, *J* = 4.5 Hz, 1H, Ph-H), 8.23 (s, 1H, N-CH). MS (ESI): 452.14 ($[M+H]^+$). Anal. Calcd for $C_{23}H_{21}N_3O_7$: C, 61.19; H, 4.69; N, 9.31; O, 24.81%. Found: C, 61.23; H, 4.51; N, 9.39; O, 24.92%.

4.2.18. 2-(2-(4-Methoxystyryl)-5-nitro-1*H*-imidazol-1-*yl*)ethyl 2,3-dihydrobenzo[*b*][1,4]dioxine-5-carboxylate (4r)

Yellow powder, yield: 65.1%. m.p. 183 ~ 185 ˚C; ^{1}H NMR (DMSO-d_6, 300 MHz, δ ppm): 3.59 (s, 3H, C-OCH_3), 4.13 (s, 4H, O-CH_2-CH_2-O), 4.65 (s, 2H, N-CH_2-C), 4.78 (s, 2H, C-CH_2-O), 6.53 (d, *J* = 4.3 Hz, 1H, C-CH-C), 7.03 (t, *J* = 4.4 Hz, 2H, C-CH-C, Ph-H), 7.22~7.44 (m, 5H, Ph-H), 7.77 (d, *J* = 6.8 Hz, 1H, Ph-H), 8.22 (s, 1H, N-CH). MS (ESI): 452.14 ($[M+H]^+$). Anal. Calcd for $C_{23}H_{21}N_3O_7$: C, 61.19; H, 4.69; N, 9.31; O, 24.81%. Found: C, 61.13; H, 4.74; N, 9.36; O, 24.87%.

4.2.19. 2-(2-(2-Chloro-6-fluorostyryl)-5-nitro-1*H*-imidazol-1-*yl*)ethyl 2,3-dihydrobenzo[*b*][1,4]dioxine-5-carboxylate (4s)

Yellow powder, yield: 54.1%. m.p. 184 ~ 186 ˚C; ^{1}H NMR (DMSO-d_6, 300 MHz, δ ppm): 4.04~4.24 (m, 4H, O-CH_2-CH_2), 4.61 (s, 2H, N-CH_2-C), 4.98 (s, 2H, C-CH_2-O), 6.57 (t, *J* = 6.9 Hz, 1H, C-CH-C), 6.90 (d, *J* = 4.3 Hz, 1H, C-CH-C), 7.0 (d, *J* = 7.83 Hz, 1H, Ph-H), 7.26~7.46 (m, 4H, C-CH-C, Ph-H), 7.85 (d, *J* = 5.4 Hz, 1H, Ph-H), 8.27 (s, 1H, N-CH). MS (ESI): 474.08 ($[M+H]^+$). Anal. Calcd for $C_{22}H_{17}ClFN_3O_6$: C, 55.76; H, 3.62; N, 8.87; O, 20.26%. Found: C, 55.84; H, 3.51; N, 8.96; O, 20.17%.

4.2.20. 2-(2-(2,4-Dichlorostyryl)-5-nitro-1*H*-imidazol-1-*yl*)ethyl 2,3-dihydrobenzo[*b*][1,4]dioxine-5-carboxylate (4t)

Yellow powder, yield: 63.5%. m.p. 190 ~ 192 ˚C; ^{1}H NMR (DMSO-d_6, 300 MHz, δ ppm): 4.37 (s, 4H, O-CH_2-CH_2-O), 4.62 (d, *J* = 5.3 Hz, 2H, N-CH_2-C), 5.02 (s, 2H, C-CH_2-O), 6.58 (d, *J* = 7.4 Hz, 1H, C-CH-C), 7.13~7.24 (m, 2H, C-CH-C, Ph-H), 7.53~7.72 (m, 6H, Ph-H), 8.21 (s, 1H, N-CH). MS (ESI): 490.05 ($[M+H]^+$). Anal. Calcd for $C_{22}H_{18}Cl_2N_3O_6$: C, 53.89; H, 3.49; N, 8.54; O, 19.58%. Found: C, 53.78; H, 3.56; N, 8.59; O, 19.54%.

4.2.21. 2-(5-Nitro-2-styryl-1*H*-imidazol-1-*yl*)ethyl 2,3-dihydrobenzo[*b*][1,4]dioxine-5-carboxylate (4u)

Yellow powder, yield: 62.7%. m.p. 173 ~ 175 ˚C; ^{1}H NMR (DMSO-d_6, 300 MHz, δ ppm): 4.23 (s, 2H, O-CH_2-C), 4.36 (s, 2H, C-CH_2-O), 4.67 (s, 2H, N-CH_2-C), 5.01 (s, 2H, C-CH_2-O), 6.67 (d, J = 4.5 Hz, 1H, C-CH-C), 7.23~7.35 (m, 6H, C-CH-C, Ph-H), 7.45~7.55 (m, 3H, Ph-H), 8.21 (s, 1H, N-CH). MS (ESI): 422.13 ([M+H]$^+$). Anal. Calcd for $C_{22}H_{19}N_3O_6$: C, 62.70; H, 4.54; N, 9.97; O, 22.78%. Found: C, 62.78; H, 4.61; N, 9.87; O, 22.83%.

4.3. Antiproliferation assay

The antitumor activities of synthesized compounds (**3a-3u** and **4a-4u**) against A549, Hela, U251, HepG-2 cell lines were evaluated as described elsewhere with some modifications. [27] Target tumor cell lines were grown to log phase in RPMI 1640 medium supplemented with 10% fetal bovine serum. After diluting to 2 ×10^4 cells mL^{-1} with the complete medium, 100 μL of the obtained cell suspension was added to each well of 96-well culture plates. The subsequent incubation was permitted at 37 ℃, 5% CO_2 atmosphere for 24 h before the cytotoxicity assessments. Tested samples at preset concentrations were added to six wells with sorbefacient as positive references. After 48 h exposure period, 40 μL of PBS containing 2.5 mg/mL of MTT (3-(4,5-dimethylthiazol-2-yl)-2,5-diphenyltet-razolium bromide) was added to each well. Four hours later, 100 μL extraction solution (10% SDS-5% isobutyl alcohol -0.01 M HCl) was added. After an overnight incubation at 37 ℃, the optical density was measured at a wavelength of 570 nm on an ELISA microplate reader. In all experiments three replicate wells were used for each drug concentration. Each assay was carried out for at least three times.

4.4. JAK3 inhibitory assay

To evaluate the effect of the compounds on JAK3 assembly *in vitro*, varying concentrations were pre-incubated with 10 μM JAK3 in glutamate buffer at 30 ℃ and then cooled to 0℃. After addition of GTP, the mixtures were transferred to 0℃ cuvettes in a recording spectrophotometer and warmed up to 30 ℃ and the assembly of JAK3 was observed turbid metrically. The IC_{50} was defined as the compound

concentration that inhibited the extent of assembly by 50% after 20 min incubation.

4.5. Flow cytometry

Cells (1.3×10^5 cells/mL) were cultured in the presence or not of novobiocin analogues at 200 μM. Nvb at the same concentration served as reference inhibitor. After treatment for 48 and 72 h, cells were washed and fixed in PBS/ethanol (30/70). For cytofluorometric examination, cells (10^4 cells/mL) were incubated for 30 min in PBS/ Triton X100, 0.2% /EDTA (1 mM), and propidium iodide (PI) (50 μg/mL) in PBS supplemented by RNase (0.5 mg/mL). The number of cells in different phases of the cell cycle was determined, and the percentage of apoptotic cells was quantified. Analyses were accomplished by a FACS Calibur (Becton Dickinson, Le Pont de Claix, France). Cell Quest software was used for data acquisition and analysis.

4.6. Docking simulations

For the molecular docking model, the three-dimensional X-ray structure of JAK3 (PDB code: 3FUP) acquired from the RCSB protein data bank (http://www.pdb.org) was selected as the template in which compound **4t** embed. All bound waters and ligands were eliminated from the protein and the polar hydrogen was added to the proteins. The docking procedure was carried out using CDOCKER protocol for receptor-ligand interactions section of Discovery Studio (version 3.5). Initially, the three-dimensional structures of the compounds in this paper were built by Chem. 3D ultra 12.0 software [Chemical Structure Drawing Standard; Cambridge Soft corporation, USA (2012)], then they were energetically minimized by using MMFF94 with 5000 iterations and minimum RMS gradient of 0.10. Molecular docking of all compounds was then performed using the Discovery Studio (version 3.5) as implemented through the graphical user interface CDOCKER protocol. CDOCKER is an implementation of a CHARMm based molecular docking tool using a rigid receptor.

4.6. QSAR model

Ligand-based 3D-QSAR approach was carried out using QSAR software of DS 3.5 (Discovery Studio 3.5, Accelrys, Co.Ltd). Among all the 21 compounds, 76.2% (that is 16) were used as a training set for QSAR modeling and the remaining 23.8% (that

is 5) were selected as an external test subset for validating the reliability of the QSAR model. The corresponding pIC_{50} values which were converted from the acquired IC_{50} (μM) were used for subsequent QSAR analysis as the response variable. All the definition of the descriptors can be seen in the "Help" of DS 3.5 software and they were calculated by QSAR protocol of DS 3.5.

Acknowledgements

References

1. Dreesen, O.; Brivanlou, A. H. *Stem Cell Reviews*. 2007, 3, 7.

2. Furqan, M.; Mukhi, N.; Lee, B.; Liu, D. *Biomarker Research*. 2013, 1, 5.

3. Verstovsek, S.; Mesa, R. A.; Gotlib, J.; Levy, R. S.; Gupta, V.; DiPersio, J. F.; Catalano, J. V.; Deininger, M.; Miller, C.; Silver, R. T.; *et al*. *New England Journal of Medicine*. 2012, 366, 799.

4. Ward, A. C.; Touw, I.; Yoshimura, A. *Blood*. 2000, 95, 19.

5. Wells, J. A.; Vos, D. A. M. *Annu Rev Biochem*. 1996, 65, 609.

6. Carter, S. C.; Smit, L. S. *Recent Prog Horm Res*. 1998, 53, 61.

7. Valentino, L.; Pierre, J. *Biochem Pharmacol*. 2006, 71, 713.

8. Machado, K. S.; Mieczkowski, J.; *et al*. *Cancer Biol Ther*. 2012, 13, 657.

9. Pedranzini, L.; Leitch, A.; Bromberg, J. *The Journal of Clinical Investigation.* 2004, 114, 619.

10. Darnell, J. E. *Natural Medicines*. 2005, 11, 595.

11. Yu, H.; Pardoll, D.; Jove, R. *Nat Rev Cancer*. 2009, 9, 798.

12. Boudyn, V.; Kovarik, J. *Europe PubMed Central*. 2002, 49, 349.

13. Goel, S.; Mani, S.; Soler, R. P. *Current Oncology Reports.* 2002, 4, 9.

14. Levitzki, A.; *Annual Review of Pharmacology and Toxicology*. 2013, 53, 161.

15. Jatiani, S. S.; Baker, S, J.; Silverman, L. R.; Reddy, P, E. *Genes & Cancer*. 2010, 1, 979.

16. Harrison, C.; Kiladjian, J. J.; Al-Ali, H. K.; Gisslinger, H.; Waltzman, R.; Stalbovskaya, V.; McQuitty, M.; Hunter, D. S.; Levy, R.; Knoops, L.; Cervantes, F.; Vannucchi, A. M.; Barbui, T.; Barosi, G. *N Engl J Med*. 2012, 366, 787.

17. Passamonti, F. *Blood*. 2012, 120, 275.

18. Mesa, R. A. *the Investigational Drugs Journal*. 2010, 13, 394.

19. Shalini, K.; Sharma, P. K.; Kumar, N. *Der Chemica Sinica.* 2010, 1, 36.

20. Molina, P.; Tarraga, A.; Oton, F. *Org Biomol Chem*. 2012, 10, 1711.

21. Pigni, M.; Brasili, L.; Giannella, M.; Giardina, D.; Gulini, U.; Quaglia, W.; Melchiorre, C. *J. Med. Chem*. 1988, 31, 2300.

22. Hou, Y. P.; Sun, J.; Pang, Z. H.; Lv, P. C.; Li, D. D.; Yan, L.; Zhang, H. J.; Zheng,

E. X.; Zhao, J.; Zhu, H. L. *Bioorganic & Medicinal Chemistry.* 2011, 19, 5948.

23. Aiba, Y.; Hasegawa, D.; *et al*. Bioorg *Med Chem Lett.* 2001, 11, 2783.

24. Pallavicini, M.; Budriesi, R.; Fumagalli, L.; Ioan, P.; Chiarini, A.; Bolchi, C.; Ugenti, M. P.; Colleoni, S.; Gobbi, M.; *Valoti EJ Med Chem.* 2006, 49, 7140.

25. Sun, J.; Li, D. D.; Li, J. R.; Fang, F.; Du, Q. R.; Qian, Y.; Zhu, H. L. *Org. Biomol. Chem.*. 2013, 11, 7676.

26. Luo, Y.; Li, Y.; Qiu, K. M.; Lu, X.; Fu, J.; Zhu, H. L. *Bioorg Med Chem*. 2011, 19, 6069.

27. Boumendjel, A.; Boccard, J.; Carrupt, P. A.; Nicolle, E.; Blanc, M.; Geze, A.; Choisnard, L.; Wouessidjewe, D.; Matera, E. L.; Dumontet, C. *J. Med. Chem*. 2008, 51, 2307.

Figure captions

Scheme 1. General synthesis of 2-(2-methyl-5-nitro-1*H*-imidazol-1-yl)ethan-1-ol derivatives (**4a-4u**). Reagents and conditions: (1) DMSO, CH_3ONa, 10 h; (2) CH_2Cl_2, TEA, 7 h; (3) DMF, K_2CO_3, reflux, overnight; (4) DMF, reflux, 4 h; (5) CH2Cl2, TEA, 8 h.

Figure 1. The canonical model of JAK/STAT signaling.

Figure 2. JAK2/1 and JAK3 inhibitors.

Figure 3. Chemical structures of 1,4-benzodioxan derivatives with powerful biological activities.

Figure 4. Molecular docking model of compound **4d**, **4f**, and **4t** with JAK3 (PDB code: 3FUP) performed by the CDOCKER protocol of Discovery Studio (version 3.5). (A). The 2D model of the interaction between compound **4d** and JAK3. (B). The 2D model of the interaction between compound **4f** and JAK3. (C). The 2D model of the interaction between compound **4t** and JAK3.

Figure 5. HELA cells were cultured in vitro treated with a gradient concentration (0, 6, 18, 54 *n*M) of **4t** for 24 h. Cells were stained by Annexin VeFITC/PI and apoptosis rate (Q2+Q3) showed in A, B, C, D was analyzed by flow cytometry.

Figure 6. Molecular docking model of compound **4t** with JAK3 (PDB code: 3FUP) performed by the CDOCKER protocol of Discovery Studio (version 3.5). (A). The 2D model of the interaction between compound **3t** and JAK3. (B). The 2D model of the interaction between compound **4t** and JAK3. (C). The 3D interaction map between compound **4t** and JAK3.

Figure 7. (A) Using linear fitting curve to compare the predicted pIC50 value with that of experiment. (B) Isosurface of the 3D-QSAR model coefficients on electrostatic potential grids. The blue triangle mesh represents positive electrostatic potential and the red area represents negative electrostatic potential. (C) Isosurface of the 3D-QSAR model coefficients on Van der Waals grids. The green triangle mesh representation indicates positive coefficients; the yellow triangle mesh indicates negative coefficients.

Table 1. Structural features, Inhibition activities (IC_{50}, μM) of compounds **3a-3u** against A549, Hela, U251 and HepG-2

compounds	R	IC_{50}(μM)			
		A549	**Hela**	**U251**	**HepG-2**
3a	*o*-F	3.01	3.35	5.75	2.74
3b	*m*-F	2.87	0.98	1.66	2.73
3c	*p*-F	3.85	1.20	2.87	1.80
3d	*o*-Cl	5.08	2.17	2.41	2.17
3e	*m*-Cl	2.94	2.41	1.71	1.24
3f	*p*-Cl	4.57	3.43	2.15	3.67
3g	*o*-Br	6.67	4.35	2.45	5.34
3h	*m*-Br	3.94	1.27	1.19	1.28
3i	*p*-Br	4.17	2.84	3.43	2.35
3j	*o*-CH_3	10.18	5.36	4.93	7.06
3k	*m*-CH_3	5.21	3.39	3.05	2.97
3l	*p*-CH_3	9.29	3.07	2.08	5.13
3m	*o*-NO_2	8.07	6.83	5.46	6.25
3n	*m*-NO_2	6.88	4.49	1.11	4.59
3o	*p*-NO_2	8.81	4.75	7.45	4.97
3p	*o*-OCH_3	9.22	1.38	3.34	3.03
3q	*m*-OCH_3	4.14	2.31	2.94	2.94
3r	*p*-OCH_3	7.15	4.46	5.86	2.99
3s	2-Cl-6-F	1.74	0.52	1.69	1.18
3t	2,4-2Cl	1.68	0.98	0.87	0.72
3u	-H	15.26	9.68	6.13	12.24

Table 2. Structural features, inhibition (IC_{50}, *n*M) of A549, Hela, U251 and HepG-2 cells proliferation and inhibition (IC_{50}) of JAK 3 by compounds **4a-4u**

compounds	R	IC_{50}(*n*M)				
		A549	**Hela**	**U251**	**HepG-2**	**JAK 3**
4a	*o*-F	108	33	132	161	15
4b	*m*-F	95	48	59	87	23
4c	*p*-F	161	53	48	118	46
4d	*o*-Cl	266	76	65	232	49
4e	*m*-Cl	101	47	74	94	31
4f	*p*-Cl	383	53	193	133	33
4g	*o*-Br	223	177	89	358	54
4h	*m*-Br	116	62	63	103	42
4i	*p*-Br	219	66	107	221	74
4j	*o*-CH_3	435	91	215	363	67
4k	*m*-CH_3	227	68	133	135	50
4l	*p*-CH_3	309	71	162	106	46
4m	*o*-NO_2	576	132	386	555	82
4n	*m*-NO_2	264	94	164	249	25
4o	*p*-NO_2	475	86	204	173	49
4p	*o*-OCH_3	231	102	75	247	52
4q	*m*-OCH_3	122	62	101	128	57
4r	*p*-OCH_3	372	18	140	111	33
4s	2-Cl-6-F	84	25	69	76	13
4t	2,4-2Cl	65	21	44	16	9
4u	-H	744	78	405	314	102
Tofacitinib citrate		114	5	27	12	1

Table 3. Experimental, predicted inhibitory activity of compounds **4a-4u** by 3D-QSAR models based on active conformations obtained by molecular docking

compounds	JAK3		Residual
	Experiment pIC50	Predicted pIC50	error
4a [a]	7.387	7.408	-0.021
4b [a]	7.319	7.427	-0.108
4c	7.292	7.239	0.053
4d	7.222	7.312	-0.09
4e [a]	7.328	7.433	-0.105
4f	7.167	7.079	0.088
4g	7.276	7.351	-0.075
4h	7.252	7.314	-0.062
4i	7.194	7.247	-0.053
4j [a]	7.018	7.115	-0.097
4k	7.207	7.135	0.072
4l	7.148	7.091	0.057
4m	6.991	6.921	0.07
4n [a]	7.027	7.16	-0.133
4o	7.065	7.124	-0.059
4p	7.284	7.235	0.049
4q	7.42	7.483	-0.063
4r	7.201	7.251	-0.05
4s	7.602	7.537	0.065
4t	7.678	7.614	0.064
4u	7.108	7.021	0.087

[a] Compounds were selected as the test sets while the rest ones were in the training sets

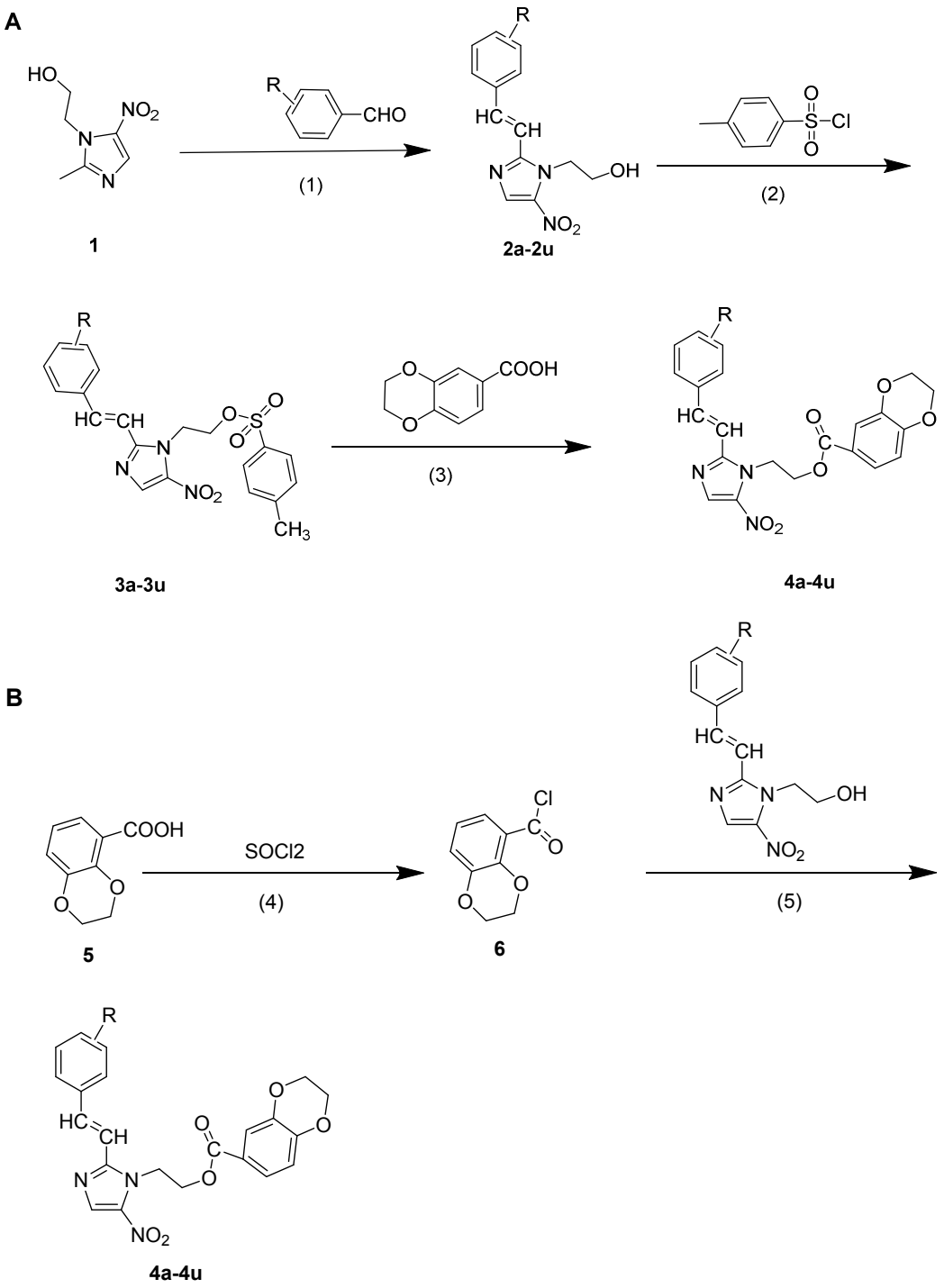

Scheme 1. General synthesis of 2-(2-methyl-5-nitro-1*H*-imidazol-1-yl)ethan-1-ol derivatives (**4a-4u**). Reagents and conditions: (1) DMSO, CH_3ONa, 10 h; (2) CH_2Cl_2, TEA, 7 h; (3) DMF, K_2CO_3, reflux, overnight; (4) DMF, reflux, 4 h; (5) CH_2Cl_2, TEA, 8 h.

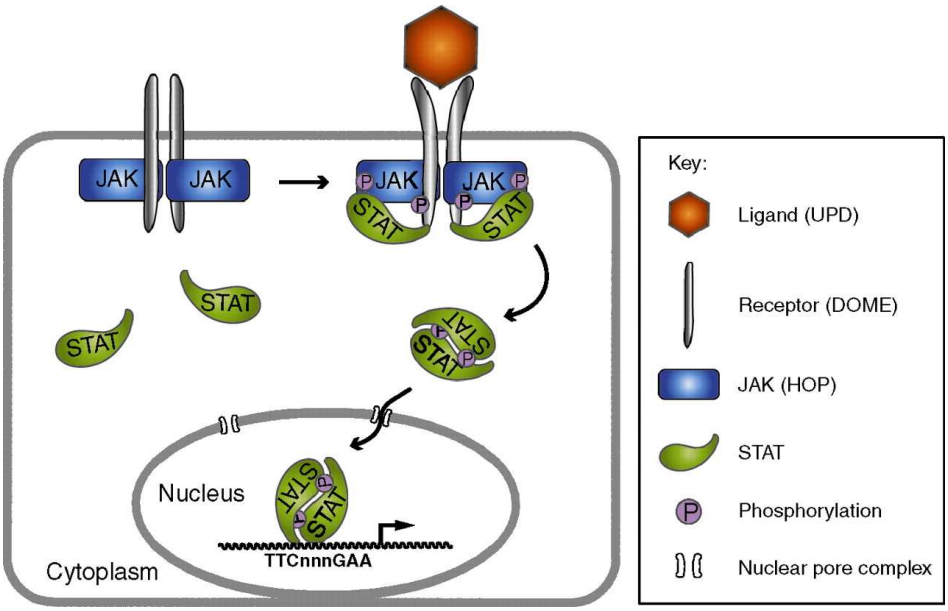

Figure 1. The canonical model of JAK/STAT signaling.

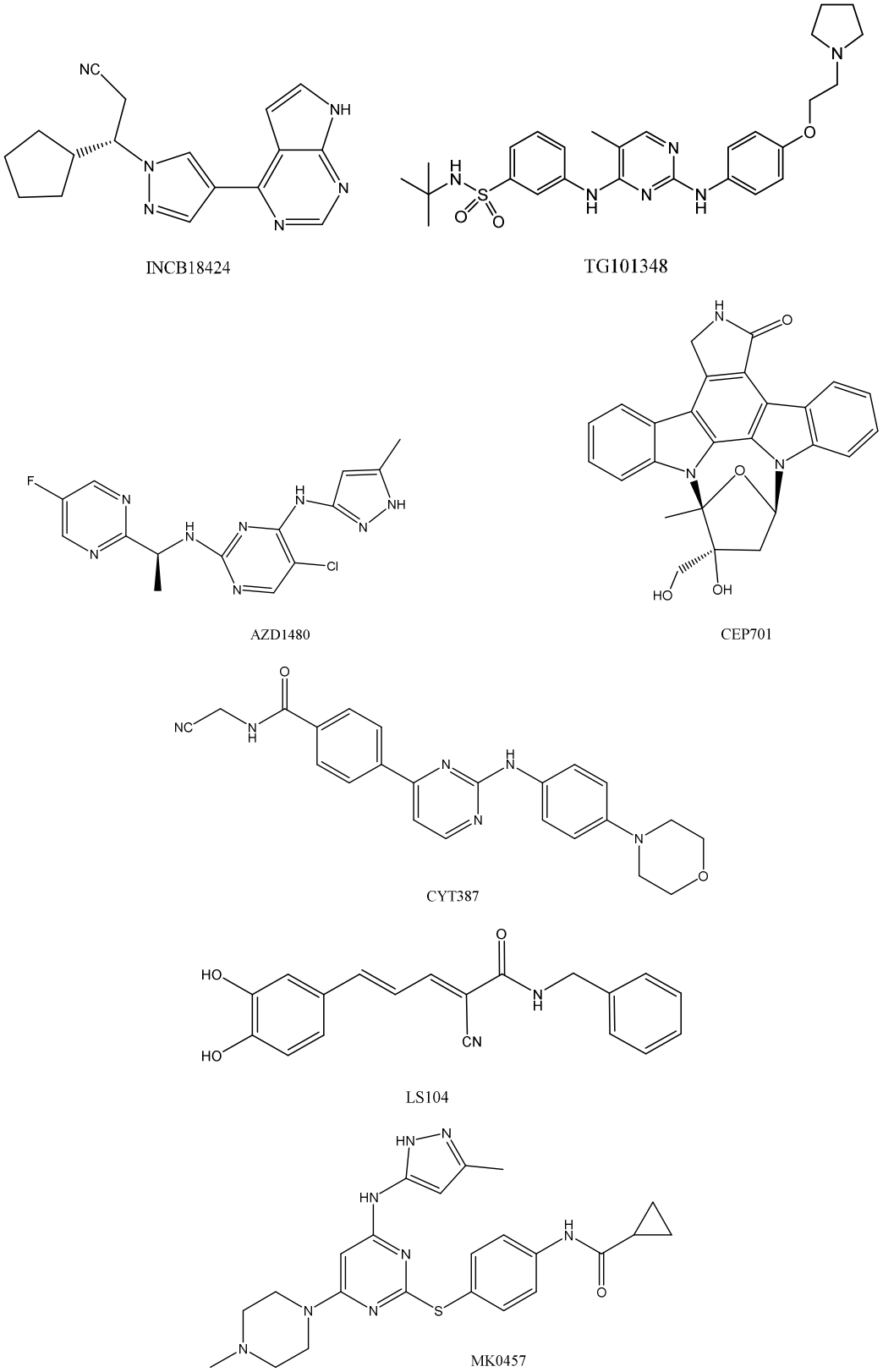

Figure 2. JAK2/1 and JAK3 inhibitors.

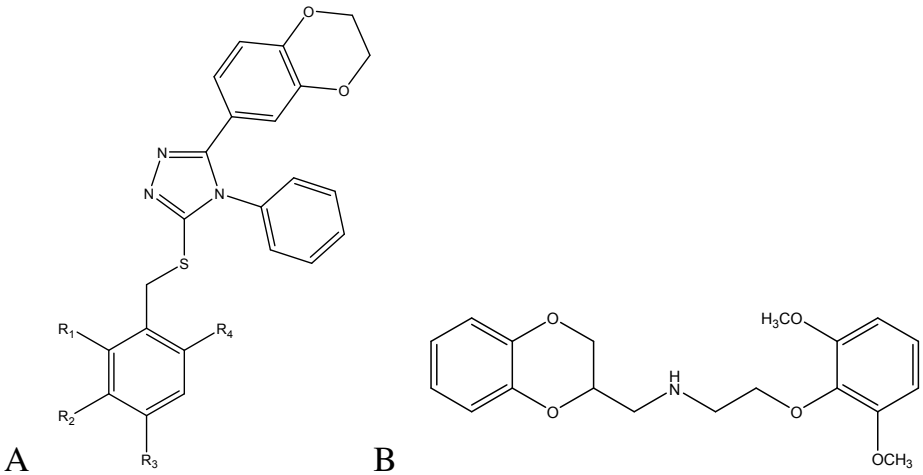

Figure 3. Chemical structures of 1,4-benzodioxan derivatives with powerful biological activities.

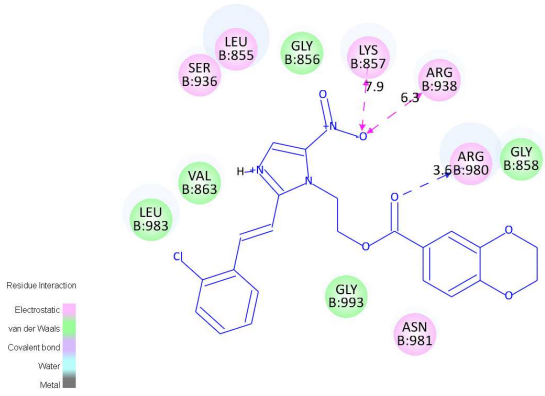

A

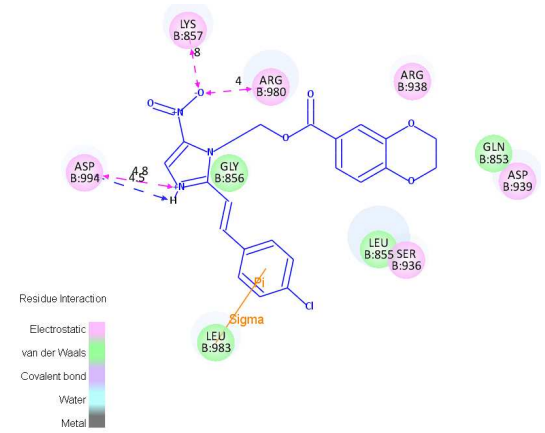

B

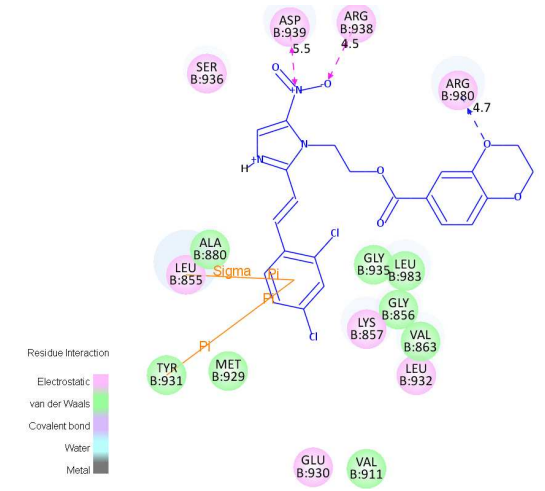

C

Figure 4. Molecular docking model of compound **4d**, **4f**, and **4t** with JAK3 (PDB code: 3FUP) performed by the CDOCKER protocol of Discovery Studio (version 3.5). (A). The 2D model of the interaction between compound **4d** and JAK3. (B). The 2D model of the interaction between compound **4f** and JAK3. (C). The 2D model of the interaction between compound **4t** and JAK3.

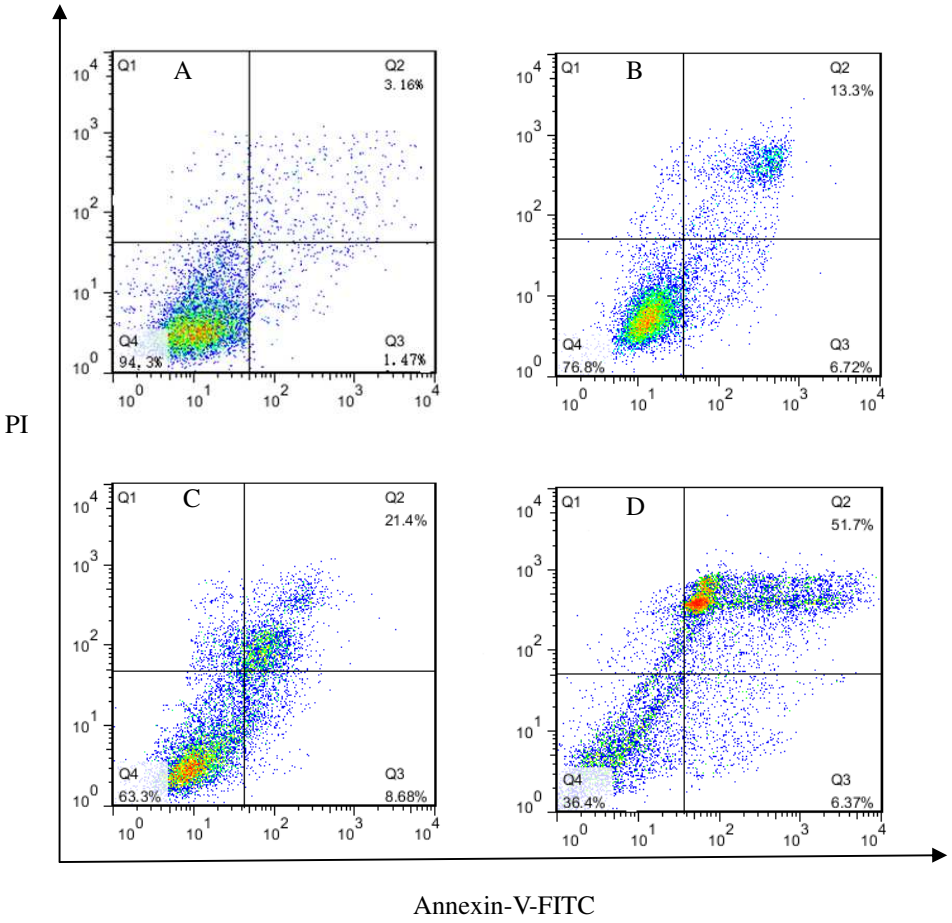

Figure 5. HELA cells were cultured in vitro treated with a gradient concentration (0, 6, 18, 54 *n*M) of **4t** for 24 h. Cells were stained by Annexin VeFITC/PI and apoptosis rate (Q2+Q3) showed in A, B, C, D was analyzed by flow cytometry.

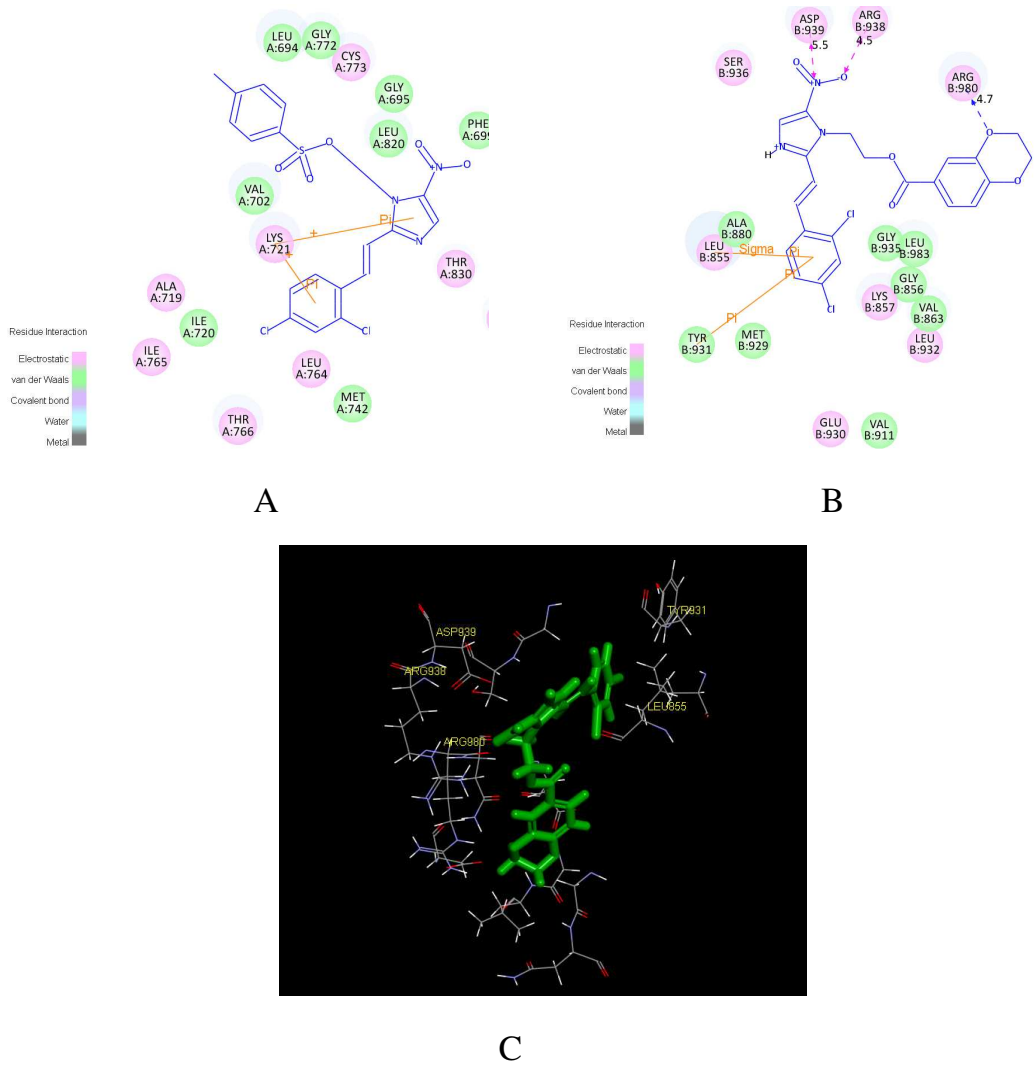

A B

C

Figure 6. Molecular docking model of compound **4t** with JAK3 (PDB code: 3FUP) performed by the CDOCKER protocol of Discovery Studio (version 3.5). (A). The 2D model of the interaction between compound **3t** and JAK3. (B). The 2D model of the interaction between compound **4t** and JAK3. (C). The 3D interaction map between compound **4t** and JAK3.

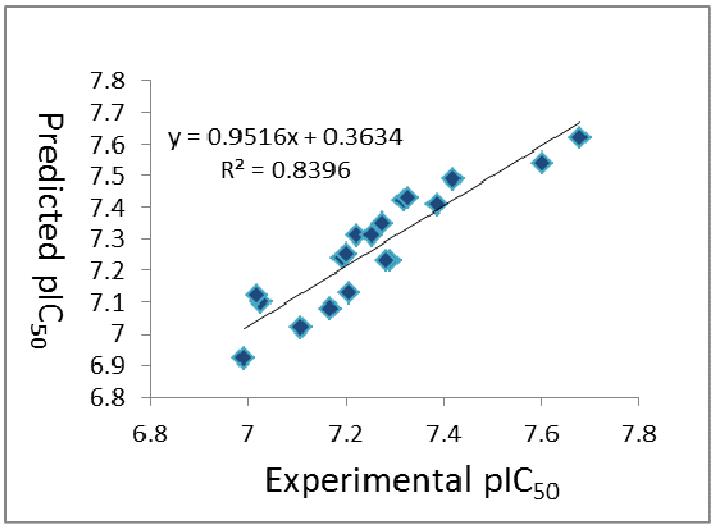

A

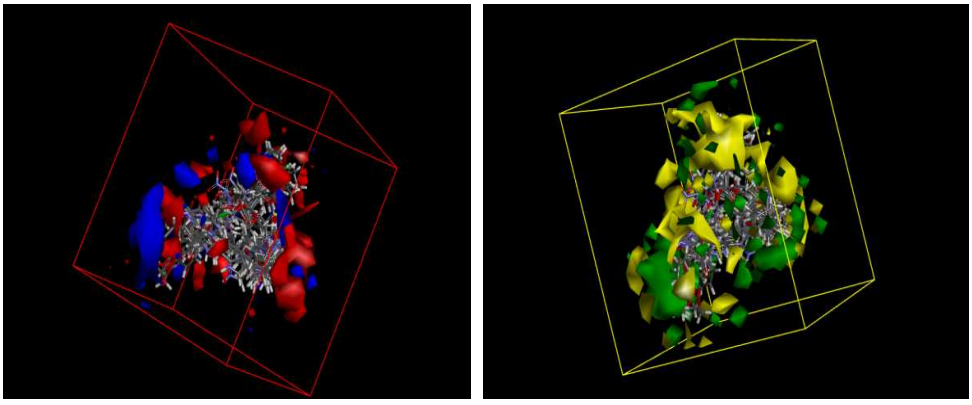

B C

Figure 7. (A) Using linear fitting curve to compare the predicted pIC50 value with that of experiment. (B) Isosurface of the 3D-QSAR model coefficients on electrostatic potential grids. The blue triangle mesh represents positive electrostatic potential and the red area represents negative electrostatic potential. (C) Isosurface of the 3D-QSAR model coefficients on Van der Waals grids. The green triangle mesh representation indicates positive coefficients; the yellow triangle mesh indicates negative coefficients.

Design, synthesis, biological evaluation and molecular docking of novel metronidazole derivatives as selective and potent JAK inhibitors

Ya-Li Sang†, Yong-Tao Duan†, Han-Yue Qiu, Peng-Fei Wang, Zhong-Chang Wang, Hai-Liang Zhu *

State Key Laboratory of Pharmaceutical Biotechnology, Nanjing University, Nanjing 210093, People's Republic of China

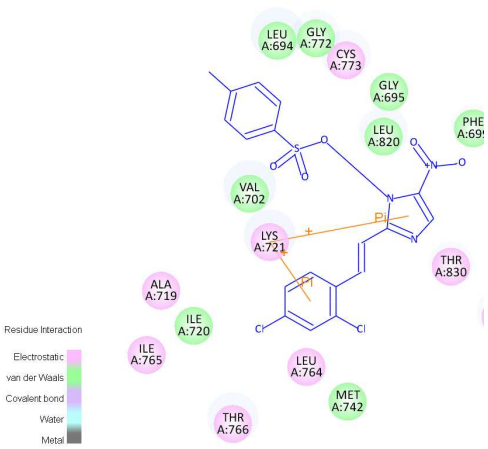

A

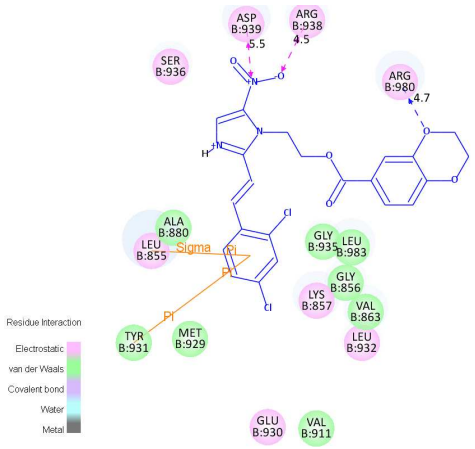

B

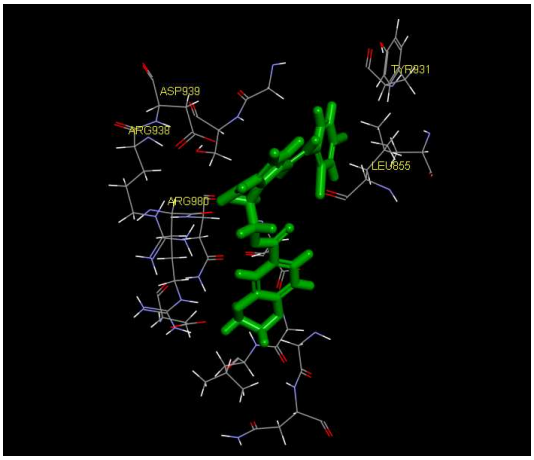

C

Two series of novel metronidazole derivatives as potential inhibitors targeting JAK have been designed, synthesized and their biological activities were also evaluated. Molecular docking models of compound **3t**, **4t** with JAK3 (PDB code: 3FUP) were performed by the CDOCKER protocol of Discovery Studio (version 3.5). (A). The 2D model of the interaction between compound **3t** and JAK3. (B). The 2D model of the interaction between compound **4t** and JAK3. (C). The 3D interaction map between compound **4t** and JAK3.